Inorganica Chimica Acta 535 (2022) 120862

Contents lists available at ScienceDirect

Inorganica Chimica Acta

journal homepage: www.elsevier.com/locate/ica

Hematite-based photoelectrochemical interfaces for solar fuel production

Serena Berardi *, Vito Cristino, Carlo Alberto Bignozzi, Silvia Grandi, Stefano Caramori

University of Ferrara, Department of Chemical, Pharmaceutical and Agricultural Sciences, Via Luigi Borsari 46, 44121 - Ferrara, Italy

ARTICLE INFO

This article is dedicated to the memory of Prof. Renato Ugo, outstanding chemist

Keywords:
Photoelectrochemistry
Hematite
Water splitting
Photoinduced oxidations
Charge carrier dynamics

ABSTRACT

The production of solar fuels, i.e. energy-rich molecules obtained from sunlight-driven processes, represents one of the most pursued strategies to satisfy the increasing global energy demand in a sustainable way. Indeed, solar energy possesses the appealing features of being abundant, inexhaustible and widely geographically distributed, yet intermittent. Thus, a common approach consists in the development of specific devices (e.g. photoelectrochemical cells, PECs) allowing for its storage in the form of chemical energy.

In order to produce viable PEC systems, the main focus should be the optimization of the light absorbing component(s), which generally comprise the exploitation of semiconductors (SCs). These materials must be efficient, durable, cheap and energetically suitable to perform the reaction(s) leading to the desired solar fuel(s). Hematite (α-Fe_2O_3) possesses these features, being composed by earth abundant elements, as well as being capable of harvesting a sizable portion of the solar spectrum. Its valence band maximum, more positive than the redox potential of water oxidation, makes it an interesting candidate for the photoinduced oxygen production *via* water splitting.

In this short review, we will mainly discuss the capitalization on hematite properties for such process, while implementing suitable optimization techniques in its synthesis (namely nanostructuring, doping and surface functionalization). Examples of case studies also from our laboratory will be discussed, in which various hematite-based interfaces are probed using advanced characterization techniques (e.g. electrochemical impedance spectroscopy and transient photocurrent analysis). These studies aimed at gaining insights into the key processes involved in the photocurrent generation, thus contributing to the rational design of future more efficient photoactive interfaces. This is a challenging goal since at present all the reported hematite-based photoanodes display performances that are far below the maximum thermodynamically attainable photocurrent (i.e. 12.6 mA/cm^2).

Finally, we will report on recent examples of hematite-based PEC systems yielding value-added organic compounds as the photoinduced oxidation products. This latter strategy, even if currently at its infancy, is believed to be a groundbreaking approach towards the production of organics exploiting sunlight energy in a sustainable electrochemical process.

1. Introduction

Hematite (α -Fe_2O_3) is an *n*-type semiconductor, which encompasses the target characteristics of a photoanodic material for water oxidation. It absorbs a significant portion of visible light (thanks to its modest band gap of ca. 2.2 eV), while having a more positive valence band maximum with respect to the H_2O/O_2 redox couple (Fig. 1a) [1].

Furthermore, hematite displays a good chemical stability in aqueous alkaline media, and it is composed of earth-abundant elements of null toxicity, thus fostering its use in a potential mass production device.

However, despite its promise, hematite has some serious limitations to cope with. First, the majority carriers display a low conductivity value (ca. 10^{-14} Ω^{-1} cm^{-1}) [3], and the minority carriers a short diffusion length (2–4 nm) [4]. These aspects, together with the slow kinetics of hole transfer to the electrolyte, contribute to reduce the charge collection efficiency over competing recombination pathways, thus limiting the photoelectrochemical performances of this material.

Nonetheless, these drawbacks can be overcome (or at least partially mitigated) by a tailored tuning of hematite properties. In the specific, synthetic strategies must be oriented towards the formation of nanostructured films, in which the particular nanoscale morphology would allow for a reduced distance for the carriers to travel in order to be

* Corresponding author.
E-mail address: brrsrn@unife.it (S. Berardi).

https://doi.org/10.1016/j.ica.2022.120862
Received 9 August 2021; Received in revised form 11 February 2022; Accepted 11 February 2022
Available online 14 February 2022

effectively collected (see Fig. 1b) [2]. At the same time, this approach should not limit the light absorption properties of the resulting material: Thus, a compromise between film thickness and morphology/size of the nanostructures should be pursued.

Alternative/complementary optimization approaches, aimed at improving hematite conduction properties, rely on the substitutional doping of its crystal structure. The introduction of tetravalent cations as electronic dopants, such as (but not limited to) Ti(IV), [5,6], Sn(IV) [7–10] and Pt(IV) [11], are usually reported to enhance the photoelectrochemical performances of the resulting hematite films by increasing the carrier concentration, as well as by causing lattice distortion leading to polaron hopping [12]. Sometimes doping strategies result in the formation of heterojunctions, which are particularly beneficial in the separation of photogenerated charges [5,6,13–15].

Finally, the oxygen evolving kinetics on hematite can be boosted through several surface modification strategies. Indeed, both the surface functionalization with water oxidation catalysts (WOCs) [7,8,16–19], and the introduction of specific layers able to passivate hematite's trap states (e.g. TiO_2 [20], Al_2O_3 [18,21,22] or Ga_2O_3 [23] thin overlayers), were extensively explored. In both cases, a cathodic shift of the photocurrent onset is generally observed, indicating that, following surface modification, the photoanode is able to produce a larger photovoltage. While the presence of a WOC is generally reported to enable hole extraction from the SC surface, enhancing spatial separation of the photogenerated charges, the introduction of thin passivating layers reduces the recombination mediated by trap states. These states originate from the truncation of the lattice at the SC surface, and are still a debated topic in the literature, [24–26] since their understanding is pivotal to understand the mechanisms of the interfacial reactions.

In this review, we will discuss some selected examples in which the abovementioned strategies were envisaged to cope with the intrinsic challenges posed by the use of hematite for solar fuel production. At the same time, some examples of the application of perturbative techniques to the investigation of charge transfer dynamics at hematite-based interfaces (e.g. electrochemical impedance spectroscopy, EIS, and transient photocurrent analysis, TPC), will be discussed.

2. Optimizing the photocurrent output in hematite photoanodes

2.1. Morphology control

One of the most common strategies for the synthesis of nanostructured hematite deals with the growth of a FeOOH phase onto transparent conductive oxides (TCO) substrates (e.g. fluorine-doped tin oxide, FTO), followed by an annealing step. The latter aims at the transformation of the deposited film into α-Fe_2O_3 phase, as well as at the sintering of the nanostructures in order to create conductive neckings among the hematite nanostructures and the FTO electron collector. The initial FeOOH growth can be obtained from suitable iron precursors via hydrothermal methods [9,10,27–29] or via electrodeposition [30,31]. These procedures lead to morphologies spanning from fused quite spherical nanoparticles [31], to rod-like nanostructures [9,27,29], to nanowires [10,28], depending on the synthetic conditions, with maximum photocurrent outputs in the range 0.5–2.5 mA/cm^2 (see Fig. 2a for an example). A recent study pointed out that ferrihydrate is converted to goethite in the initial stages of hematite hydrothermal synthesis [32]. The α-Fe_2O_3 phase is then formed upon dehydration of the goethite.

Alternatively, Fe_2O_3 sols (obtained from $FeCl_3$ hydrolysis or from preformed particles) containing a porogen can be spread (e.g. spin-coated or doctor bladed) onto the TCO substrate [7]. After the porogen is burned in a specific high temperature annealing step, the resulting films consist of an interconnected hematite particle film having a porous morphology. Preformed Fe_2O_3 nanoparticles can also be deposited via electrophoresis, provided the in situ generation of H^+ ions and the subsequent protonation of hydroxyl groups on the particles' surface in order to impart a net positive charge to their surface [35].

It is worth noting that the abovementioned aqueous-based synthetic methods are often limited by the formation of grain boundaries in the resulting films, which introduce recombination centers hampering the overall photoelectrochemical performances of the hematite electrodes. At the same time, when the annealing temperature is kept below 800 °C, the resulting film can display a nonstoichiometric composition (with the respect of the α-Fe_2O_3 phase) due to the residual presence of hydroxyl groups or oxygen vacancies [36]. This issue can be overcome by providing a short (usually < 20 min) annealing step up to 800 °C. Besides eliminating the excess –OH groups from the surface of hematite,

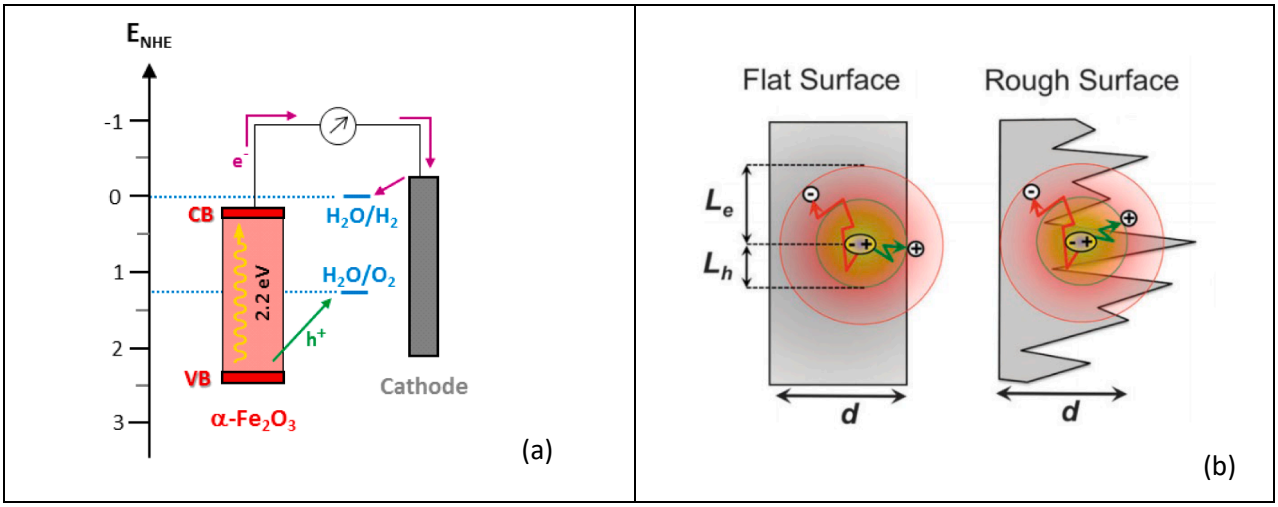

Fig. 1. (a) Energy diagram for photoelectrochemical water splitting with a hematite photoanode performing water oxidation and a cathode evolving hydrogen from water reduction. Data reported vs the Normal Hydrogen Electrode, NHE. (b) Schematic representation of charge collection in flat vs nanostructured (rough) surfaces. L_e and L_h are respectively the electron and hole diffusion lengths, while d is the thickness. In the rough/porous material at the right side of Fig. 1b, the path for hole injection into the electrolyte can be shorter than $L_h = (D_h \cdot \tau_h)^{1/2}$, where D_h and τ_h are the hole diffusion coefficient [cm^2/s] and lifetime respectively. Once holes are scavenged, electrons are virtually free to diffuse/migrate without recombination to the ohmic collector. Reproduced with permission from [2] (Copyright 2015, Springer International Publishing Switzerland).

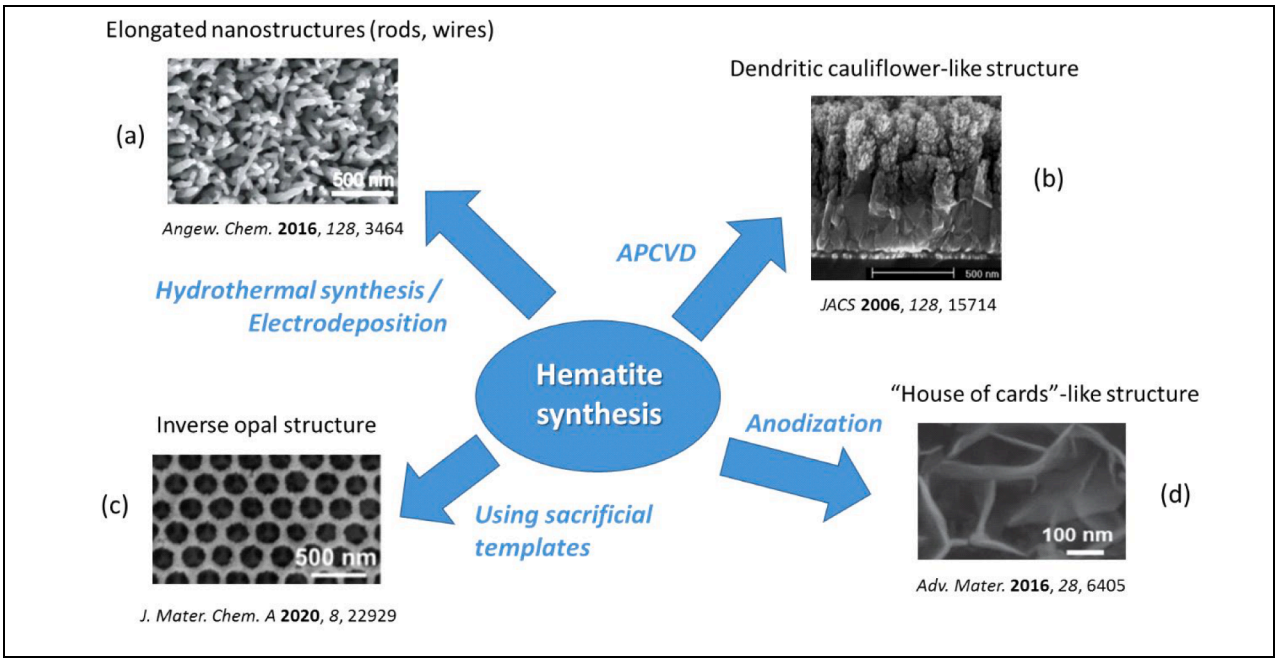

Fig. 2. Some of the most successful synthetic routes affording different nanostructured hematite thin films aimed at optimizing charge separation and electrolyte percolation through the porous semiconductor network. SEM micrographs are reproduced with permission from [28] (Copyright 2016, John Wiley & Sons), [33] (Copyright 2006, American Chemical Society), [34] (Copyright 2020, Royal Society of Chemistry) and [29] (Copyright 2016, John Wiley & Sons).

which behave as recombination centers, this procedure enables a partial migration of Sn(IV) ions from the underlying substrate (when FTO is used), which ends up acting as a *n*-type dopant in the resulting film, creating oxygen vacancies. This unintentional doping certainly reduces the overall conductivity properties of the TCO itself, thus a compromise in the annealing conditions must be found. At the same time, the high-temperature treatment usually leads to a coalescence of the original nanostructures, resulting in larger domains, deleterious for the charge mobility. Encapsulation strategies, based, for example, on the introduction of a SiO_2 confinement scaffold on the top of the hematite film prior to its 800 °C-annealing, have been proposed [37], being effective in the retention of the features' size once the SiO_2 is removed. The resulting electrodes showed an almost doubled performances in terms of maximum photocurrent (up to 2.3 mA/cm^2 at 1.43 V vs RHE [**]) with the respect to the non-encapsulated 800 °C-annealed photoelectrodes [37].

At the same time, more sophisticated growing techniques have been explored, through which a less-defective hematite crystalline phase can be obtained. In particular, the Graetzel group reported on the synthesis of a dendritic hematite nanostructured via the atmospheric pressure chemical vapour deposition (APCVD) of $Fe(CO)_5$ in the presence of tetraethyl orthosilicate (the latter acting as a source of Si(IV) dopant) [33]. The resulting cauliflower-like structure display feature size as low as 5–10 nm at the semiconductor-liquid junction (see Fig. 2b), thus yielding maximum photocurrent values up to 1.8 mA/cm^2 at 1.23 V (3 mA/cm^2 at 1.6 V). At the same time, the thick lower parts of this structure guarantee that a good portion of the solar spectrum is indeed absorbed by the film (42% IPCE at 370 nm under 1.23 V) [22]. It is worth noting that this synthetic procedure resulted in high-quality hematite films prepared at temperatures as low as 450 °C: a better crystallinity is thus obtained without the 800 °C annealing step. Later, these cauliflower-like electrodes were further optimized by fine tuning the heater set temperature and air-flow rate, yielding up to 4.0 mA/cm^2 at 1.53 V (ca. 2.3 mA/cm^2 at 1.23 V) [38]. Dark field transmission electron microscopy and conducting atomic force microscopy analyses evidenced that in these optimized photoanodes the 82% of the nanoparticle aggregates possess different crystallographic orientations, each one extended for large areas. Thus, the resulting interface contains a low amount of high-angle grain boundaries, which usually act as recombination centers or can generate a potential barrier hindering the majority carrier transport between adjacent crystals [39].

Laying aside techniques requiring expensive instrumentation, engineered morphology with nanostructured domains can be also obtained via solution processed synthetic methods, providing the prior introduction of sacrificial templating materials. For example, the Sivula group reported on the formation of a copper-iron oxide phase via a sol–gel synthesis, followed by controlled annealing procedures and treatment with NaCl [40]. Interestingly, the procedure yielded a pure hematite phase: Thus, the authors speculated that the annealing in the presence of NaCl lead to a coalescence of Fe_2O_3 grains, which grow following the orientation given by the CuO phase, the latter thus acting as a template. At the same time, CuO segregates and reacts with NaCl, producing volatile compounds (CuCl and Na_2O_2), swept away by the carrier gas in the tubular oven. The performances of the resulting hematite photoanodes are considerable, resulting in a ca. 2 mA/cm^2 photocurrent density at 1.6 V.

Among the synthetic procedures involving the use of templates, very promising results were obtained from the formation of a regular array of polymer spheres on top of the FTO electrode. After the infiltration of ferric ions in the interstitial voids created between these polymer spheres (under proper temperature and humidity conditions), a FeOOH layer can be grown upon Fe^{3+} hydrolysis in order to generate (after calcination and template removal) a regular inverse opal (IO) structure, consisting of fused 20–30 nm hematite particles (see Fig. 2c) [34]. This peculiar morphology allows for an enhanced absorption thanks to the resulting crack-free periodic structure (photonic crystal) [41,42]. At the same time, the intrinsic porosity ensued a large area exposed to the electrolyte, yielding up to ca. 7 mA/cm^2 photocurrent density at 1.5 V

[*] Unless otherwise stated, all the potential values given in this review are reported versus the reversible hydrogen electrode, RHE.[†] Further permissions related to the material excerpted should be directed to the American Chemical Society, https://pubs.acs.org/

(>2 mA/cm^2 at 1.23 V) for the optimized IO-hematite photoanodes. The corresponding IPCE value, registered at 1.23 V, is 19.3% at 380 nm.

Hematite nanostructures can be also synthesized using a "top-down" approach, e.g. via the electrochemical anodization of an iron foil. This potentially easy to scale method implies the application of a highly positive voltage to a metallic Fe electrode, in the presence of "templating" ions (e.g. fluorides), helping to etch the foil surface into peculiar Fe_2O_3 nanostructures. For example, the Wang group reported on a specific anodization leading to vertically aligned hematite nanosheets (200 nm lateral size and 600 nm height in average), interconnected in a "house of cards"-like structure (see Fig. 2d) [43]. This peculiar morphology lead to > 5 mA/cm^2 photocurrent density at 1.6 V, which can be further enhanced (up to 7 mA/cm^2) by introducing Ag nanoparticles and cobalt phosphate (CoPi) cocatalyst. The resulting heterointerface display a reduced charge transfer resistance of the photoanode, probably due to improved hole transfer through the CoPi layer, while it is believed that the Ag nanoparticles provide a plasmonic effect, enhancing both light harvesting and charge separation. All the above mentioned strategies for hematite synthesis can be further refined in order to introduce dopant ions, as it will be discussed in the following section.

2.2. Doping strategies

Doping is a commonly used strategy aimed at increasing the majority carrier concentration, thereby improving the semiconductor conductivity. In particular, hematite photoanodes are frequently doped via the incorporation of tetravalent cations, such as Ti(IV), Sn(IV) or Pt(IV). For example, the effect of Pt(IV) doping on electrochemically deposited hematite was studied [11]. A remarkable photocurrent density of 1.43 mA/cm^2 at 0.4 V vs Ag/AgCl was achieved for the 5% Pt-doped sample, almost doubling the performances of the bare hematite counterpart. This enhancement was attributed to the increased donor density and conductivity, as well as to the deeper Schottky barrier, whose magnitude scales linearly with the doping density, which in turns improve the charge separation efficiency. It is worth noting that higher concentrations of the Pt(IV) dopant lead instead to worse photoanodic performances, due to the formation of highly dense recombination centers.

As an alternative strategy, P(V) doping has been recently reported to provide enhanced electron mobility, together with a higher number of carriers [44]. The resulting photoanodes yield up to 2.7 mA/cm^2 photocurrent at 1.23 V. Another feasible doping approach is the self-doping by oxygen vacancies, whose concentration is reported to greatly influence the photocurrent onset [45]. These kind of vacancies act as shallow donor dopants in hematite, thus increasing the majority carrier density and, hence, the semiconductor conductivity [12].

Alternatively, hematite can be doped with group II cations, such as Ca^{2+} or Mg^{2+}, resulting in a p-type conductivity behavior. When this kind of doping only involve the superficial layers of hematite, leaving the bulk unaffected, a *n*-p junction can be formed, in which the created built-in internal field enhances charge separation, and consequently the photoinduced activity. For example, Liu and coworkers recently reported on the formation of a *n*-p homojunction based on Fe_2O_3/Ca-doped Fe_2O_3 via a straightforward hydrothermal method. The resulting internal electric field assists the photoinduced charge separation, leading to 2.14 mA/cm^2 at 1.23 V. Furthermore, when a Pt electron collector was placed below the hematite layer and cobalt phosphate (CoPi) hole extractor on the surface of the homojunction, a further improvement of the separation was observed, with consequent enhancement of the photocurrent up to 2.94 mA/cm^2 at 1.23 V [19].

In some cases, the doping of hematite photoanodes results in the formation of new mixed metal oxide phases. One example is the formation, upon Ti(IV) doping, of iron titanates, yielding heterointerfaces having an impact on the charge transfer properties of the semiconductor/electrolyte junction. For example, the Andreu group reported that Ti(IV) treatment of hematite leads to the formation of a Fe_2TiO_5 phase at the SC/liquid junction [5]. Being the conduction and valence bands of this pseudobrookite phase properly aligned with hematite ones (see Fig. 3a), a cascade of charge transfer processes can take place in the resulting *n-n* Fe_2O_3/Fe_2TiO_5 heterojunction, reducing recombination and leading to a 15-fold increased performances (up to 1.3 mA/cm^2 at 1.23 V) with the respect of the bare Fe_2O_3 photoanode. The same kind of heterojunction was reported to form also starting from hematite nanowires [13]. This particular nanostructure was further functionalized with a CoFe Prussian blue analogue as the WOC, leading to a photoanode able to deliver up to 1.25 mA/cm^2 at 1.23 V in acidic media at pH 1 (almost one order of magnitude higher than the bare Fe_2O_3 nanowires). This is attributed to a modification of the electronic levels of hematite's surface states, leading to a kinetically favorable interfacial hole transfer. Furthermore, the registered photocurrent experienced only an initial drop within the first 2 h of activity, but then retained the 80% of the value in a 24 h test.

Recently, our group reported that, according to a different synthetic methodology, the incorporation of Ti(IV) ions in hematite-based photoanodes resulted in the formation of an ilmenite ($FeTiO_3$) phase at the surface [6]. As it will be discussed later, even if the energy positioning of the hematite valence band (VB) edge does not favor hole transfer to the ilmenite VB (see Fig. 3b), we could demonstrate that the formation of a thin α-$Fe_2O_3/FeTiO_3$ heterojunction both passivates deep surface traps acting as recombination centers, and supports a stronger depletion layer at the SC/electrolyte interface, which assists photoinduced charge separation.

2.3. Surface functionalization of hematite with water oxidation catalysts: The pivotal formation of adaptive junctions

In the pursuit for hematite-based photoanodes with enhanced photocurrent outputs at lower applied bias, the functionalization of the electrodic surface with suitable water oxidation catalysts (WOCs) is among the most frequently adopted strategies. As already mentioned in the Introduction, the WOC effect should translate in a cathodic shift of the photocurrent onset with the respect to the unmodified photoanodes, thus enabling photocurrent generation at low applied bias, i.e. in a region where recombination pathways prevail in the absence of the catalyst, due to the weaker depletion layer. An enhancement of the photocurrent value is often registered also at anodic bias.

The most commonly used catalysts include iron oxyhydroxide [6,8,9,46] cobalt oxide, [19,33] ruthenium and iridium oxides [47], as well as mixed-metal oxides (e.g. nickel–iron oxide [7,17,48] and copper-cobalt oxide [18], among the others). A comprehensive review of all the explored WOCs goes beyond the scope of this work, but a recent summary was reported by Souza and coworkers [16].

The introduction of a WOC on hematite surface must account for some important factors, in order not to jeopardize the photoelectrochemical performances of the resulting electrode. In the specific, an adaptive junction must be formed between the semiconductor absorber (hematite in our case) and the WOC, while the formation of buried junction must be avoided. Indeed, a buried SC/WOC junction is formed when a compact catalytic layer (e.g. crystalline IrO_2 [49]) is introduced on the SC surface, yielding a constant built-in potential (Φ_b, see Fig. 4a-b), whose value is limited by the catalyst's work function (E_{WOC}).

On the other hand, the SC functionalization with porous catalysts (e.g. $Ni(OH)_2$ [49]) will results in a so-called adaptive SC/WOC junction (Fig. 4c-d), enabling the hole transfer from the illuminated semiconductor to the catalyst, and from the latter to the electrolytic solution. Indeed, porous and permeable WOCs display an extended density of states (DOS), allowing the charge build-up to be compensated by migration of ions from the electrolytic solution. These changes in the WOC average oxidation state result in a variable position of the Fermi level, which in turn lead to a higher barrier height ($\Phi_{b,eff}$), an increased open-circuit photovoltage and lower recombination [49]. It is worth

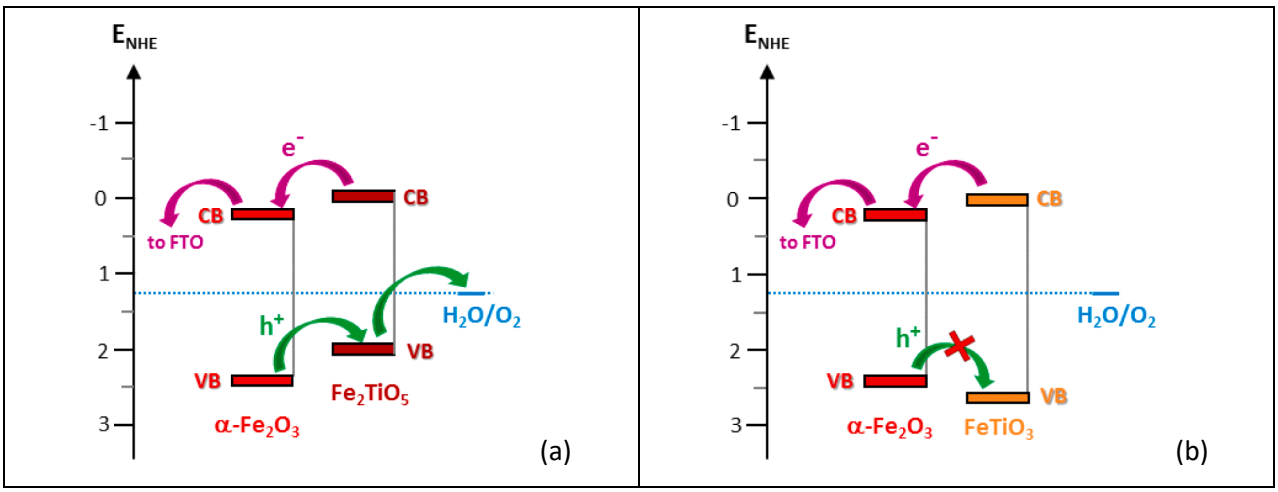

Fig. 3. Electrochemical potential diagram for α-Fe_2O_3/Fe_2TiO_5 (a) and α-Fe_2O_3/$FeTiO_3$ (b) heterojunctions. Potential values are reported vs the Normal Hydrogen Electrode (NHE) scale.

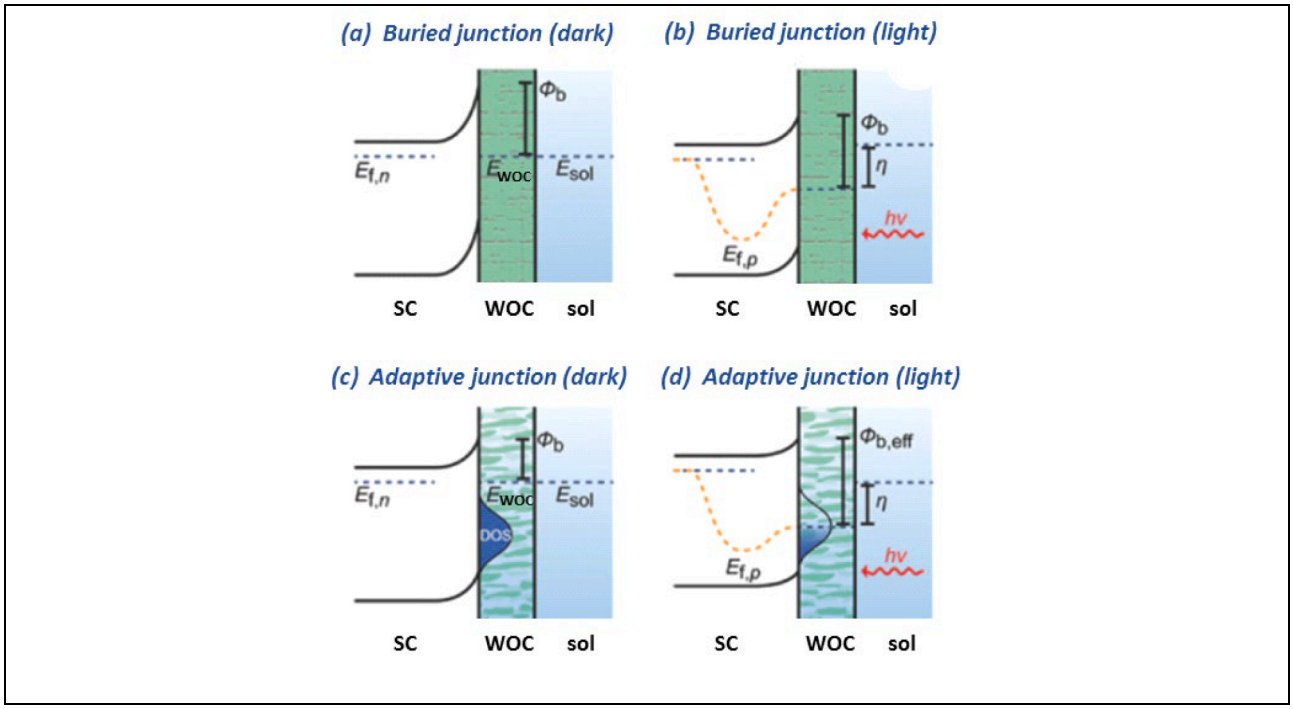

Fig. 4. Energy diagrams of different SC/WOC interfaces, yielding either a buried junction (a-b) or an adaptive junction (c-d). In d, upon illumination a larger photovoltage is produced as a result of the larger energy barrier at the interface, given by the difference between the quasi-Fermi level of the catalyst ($E_{f,p}$) and the conduction band edge of the semiconductor. Reproduced with permission from [50] (Copyright 2018, John Wiley & Sons).

noting that the WOCs should also display low absorbance values, in order to avoid a significant parasitic light absorption in the case of electrolyte-side illumination of the photoanode.

We have recently reported on the importance of this aspect, by comparing the performances of thin layer hematite (HTL) electrodes functionalized with WOCs with the same chemical composition but different morphology [8]. In particular, these WOCs were prepared by pulsed laser deposition (PLD), an easily scalable fabrication technique allowing for a versatile control of the deposited film morphology at the nanometric scale. Indeed, by changing the deposition conditions (in particular the temperature of the target) and the post-annealing temperature, we could obtain amorphous iron(III) oxide catalysts having identical nominal composition but with morphologies ranging from a porous assembly of nanoparticles (p-Fe) to a dense compact layer (d-Fe). Hematite photoanodes functionalized with the two different WOCs were tested, confirming that significantly better performances in terms of both maximum photocurrent and onset potential are obtained only with the porous catalyst (see Fig. 5a). Indeed, when compared with the bare hematite, which yields up to 0.55 mA/cm^2 maximum photocurrent, the modified interface displays a ca. 200 mV cathodic onset shift and an almost doubled photocurrent (up to ca. 1 mA/cm^2). On the other hand, hematite electrodes decorated with the compact WOC experience a significant decay of the overall performances, with<0.2 mA/cm^2 maximum photocurrent.

We have later extended this study considering the functionalization of Sn-doped thin layer hematite (SnHTL) photoanodes with other earth-abundant, non-precious, metal oxide WOCs [7]. In particular, we chose amorphous nickel–iron mixed oxides (among the best WOCs in alkaline

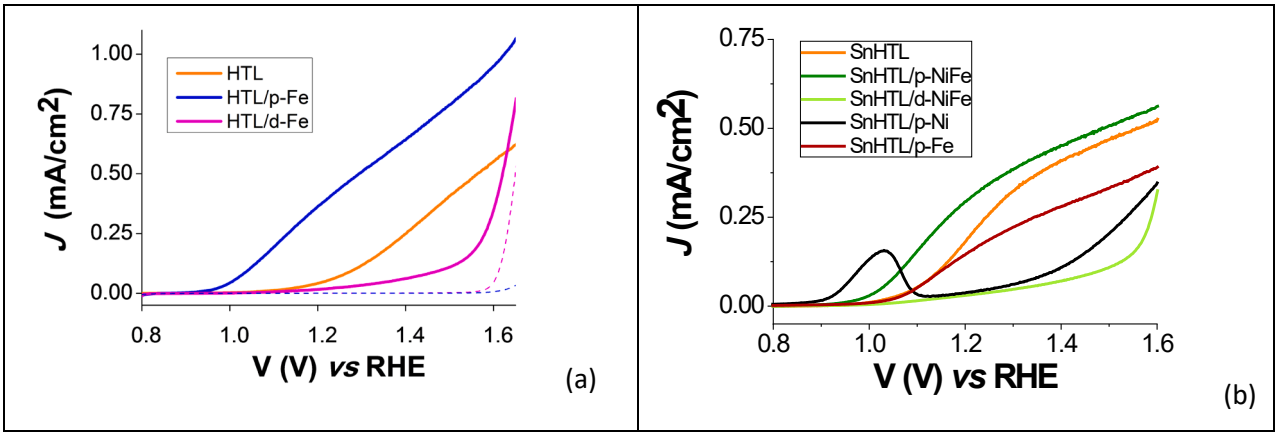

Fig. 5. (a) J-V curves of HTL photoanodes, either bare or functionalized with porous/dense iron-oxide WOC, recorded in 0.1 M NaOH under 1 sun (0.1 W/cm^2 AM1.5G) illumination. Dark scans are also reported as dashed lines. Reproduced with permission from [8] (Copyright 2016, American Chemical Society†) (b) J-V curves of SnHTL photoanodes, either bare or functionalized with porous/dense single/mixed iron/nickel-oxides recorded in purified 0.1 M KOH under 1 sun (0.1 W/cm^2 AM1.5G) illumination. Adapted with permission from [7] (Copyright 2019, American Chemical Society†).

conditions [51]) and compared them with their single-metal oxide counterparts. All catalysts were synthesized by PLD, tailoring the deposition/post-annealing parameters in order to obtain either a porous or a dense morphology. Fig. 5b summarizes the results, evidencing that the functionalization with the porous iron-nickel oxide (p-NiFe) leads, as expected, to an enhancement of the photoanodic performances, both in terms of onset (100 mV shift with the respect of bare hematite) and overall photocurrent (up to 0.6 mA/cm^2). On the other hand, when coupled with the dense iron-nickel oxide (d-NiFe), the hematite electrode performances decline significantly (ca. 0.1 mA/cm^2 at 1.5 V, value after which the dark current starts to build up). The same detrimental outcome is obtained when the dense single-metal oxide counterparts are introduced (data not shown). Instead, hematite functionalization with the porous pure nickel (p-Ni) and pure iron (p-Fe) oxides does not yield the expected improved performances. In the former case, this behavior can be ascribed to the lower intrinsic electrocatalytic activity of pure nickel oxides with respect to the mixed nickel–iron oxides [46,52], affecting the process of charge transfer to the electrolyte (see next paragraph for a detailed comment based on EIS data). On the other hand, the modified SnHTL/p-Fe interface does not yield an appreciable shift of the photocurrent onset, nor the expected enhancement of the photocurrent maximum value. This can be possibly due to different surface properties of the SnHTL vs the undoped HTL photoanode of the previous work [8], leading to a different p-Fe coverage during the PLD process. This fact can translate in the local formation of p-Fe conglomerates with low intrinsic electrical conductivity [52], resulting in a voltage drop that limits the interfacial reaction of oxygen production.

The formation of an adaptive junction between hematite and a mixed iron/nickel oxide WOC (namely $Ni_{0.8}Fe_{0.2}O_x$) was reported also by the Boettcher and Hamann groups [48]. The intrinsic properties of the resulting interface were studied using a dual working-electrode for the in situ measurement of the variation of the WOC potential upon changing the bias applied to the SC. Provided that conformal and crack-free films are used, the authors showed that the $Ni_{0.8}Fe_{0.2}O_x$ layer can harvest up to 95% of the holes generated within hematite under water oxidation conditions, thus demonstrating the role of the WOC as a hole collector.

The importance of realizing a correct alignment between the energy levels of hematite and the selected WOC was recently discussed from a computational point of view, using cobalt hexacyanoferrate (CoFe-PB) as the catalyst [14]. Density functional theory (DFT) calculations revealed an intrinsic mismatch between the two materials, resulting in a slightly uphill hole transfer from hematite's VB to the catalyst. Nonetheless, a 0.3 V cathodic shift in the experimental photocurrent onset was observed when the SC surface was functionalized with the WOC. This improvement of the performances was attributed to a shift of surface states to a lower potential occurring upon CoFe-PB deposition and under an applied bias. In these conditions, the hole transfer to the WOC is possible (leading to the formation of $Co^{III}Fe^{III}$ states), as evidenced from the cathodic shift of the maximum value of surface state capacitance.

All together, these results confirmed the importance of planning synthetic strategies in order to obtain the desired kind of SC/WOC junction. Functionalization of hematite-based photoanodes with molecular water oxidation catalyst has also been proposed, but this strategy is still at its infancy and thus it will not be described in this review.

In summary, in view of their use in viable PEC devices, it is necessary to optimize hematite-based photoanodes in order to attain high photocurrent outputs at low applied bias, following the strategies described in this paragraph (which can be certainly applied also to other SCs [53]). Furthermore, to the same end, cheap and sustainable synthetic methodologies should be preferred, together with stable and long-term operating materials.

3. Addressing the charge transfer dynamics in hematite-based interfaces: Some case studies

The exploitation of the full-potential of hematite to perform as a photoanode for water oxidation is hampered by the still limited knowledge about both the interfacial energetics and density of states of the illuminated semiconductor and the charge transfer dynamics occurring under the operational conditions of the photoanode. To fill this gap, several advanced techniques started to be quite routinely employed in the characterization of hematite-based interfaces. Among them, the electrochemical impedance spectroscopy (EIS) attracted particular attention, since it can provide information on processes with different characteristic time constants, such as charge transport/trapping/transfer. Indeed, by applying a small sinusoidal perturbation (usually 10–20 mV) superimposed to the bias potential, and varying its frequency, the frequency response of the photoelectrode as a function of the voltage can be modeled, and the value of specific circuital elements (i.e. resistances and capacitances) obtained. In particular, one of the most commonly used circuit models for rationalizing the output of EIS experiments on nanostructured hematite electrodes is reported in Fig. 6a [8,26]. The nested mesh accounts for the resistance and capacitance of the space charge layer (respectively R_{SC} and CPE_{SC}, being CPE the constant phase element, i.e. a non ideal capacitance), as well as for the interfacial charge transfer resistance and capacitance (R_{CT} and CPE_{CT}).

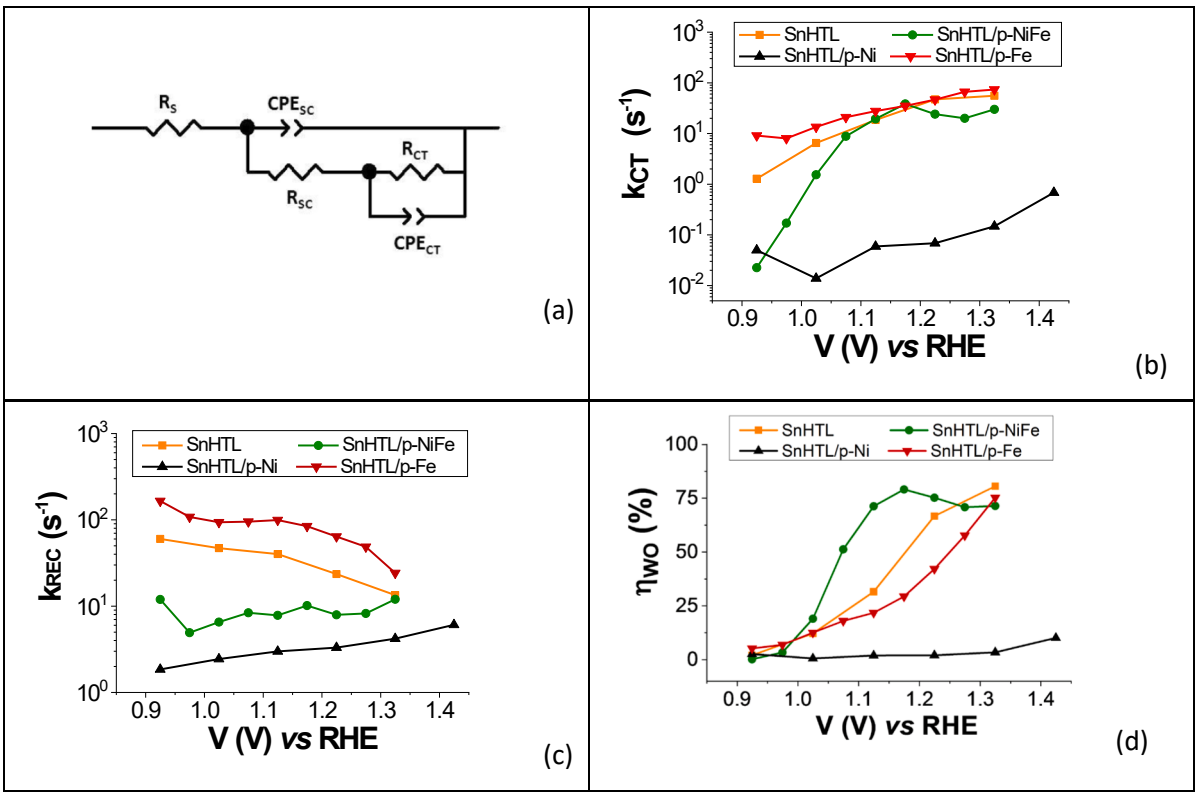

Fig. 6. (a) Equivalent circuit commonly used to fit EIS data of hematite-based photoanodes. (b – d) Rate constants associated to charge transfer (k_{CT}, in b) and recombination (k_{REC}, in c) and water oxidation efficiency (η_{WO}, in d) for SnHTL (orange squares), SnHTL/p-NiFe (green circles), SnHTL/p-Ni (black triangles), and SnHTL/p-Fe (wine reverted triangles). Data extracted from EIS experiments recorded in purified 0.1 M KOH under 1 sun illumination (0.1 W/cm^2 AM1.5G). Adapted with permission from [7] (Copyright 2019, American Chemical Society†).

More specifically, the CPE_{CT} value is related to the transfer of holes trapped in bare hematite's surface states, while for the WOC-functionalized interfaces it is associated to hole accumulation into catalyst's states, prior to their transfer to the electrolyte. The R_{SC} and CPE_{SC} are thus related to the high-frequency impedance values, while R_{CT} and CPE_{CT} correspond to the low-frequency region, being slower processes.

For example, the comparative EIS study allowed us to gain important insights on the dynamics of charge transport/transfer on the previously described single/mixed metal oxide-functionalized SnHTL photoelectrodes [7]. The analysis of EIS data aimed at calculating the rate constants of (i) the charge transfer to the electrolyte (k_{CT}), and (ii) the k_{REC} of e^-/h^+ recombination at the electrode's surface, following the procedures reported by Peter *et al.*, [54] and later implemented by Mendes *et al.* [47] These two rate constants can be properly combined in order to determine the photoelectrochemical water oxidation efficiency (η_{WO}), according to the formula: $\eta_{WO} = \frac{k_{CT}}{k_{CT}+k_{REC}}\%$.

When analyzing the k_{CT} and k_{REC} trends for the different interfaces (Fig. 6b and c), the primary processes limiting the overall performances (η_{WO}, Fig. 6d) of the different electrodes can be evidenced and rationalized. In the following examples, we focus the discussion only on the porous WOCs, since with their compact counterparts the hole transfer to the electrolyte is hampered, severely limiting the overall performances of the resulting photoanodes.

As far as the SnHTL/p-Ni photoanodes are concerned, from the abovementioned analysis we could assess that the poor photoelectrochemical output showed in Fig. 5b, is mainly due to the slow charge transfer to the electrolyte (k_{CT} values < 1, see Fig. 6b). This can be ascribed to the lower intrinsic electrocatalytic activity of pure nickel oxides with respect to the mixed nickel–iron oxides [46,52], which in the end severely hamper the photocurrent generation, even if at the same time the SnHTL/p-Ni interfaces possess the lowest recombination rate. On the other hand, in SnHTL/p-Fe photoanodes a high charge transfer rate is accompanied to a high recombination rate, the latter causing greater recombination losses with respect to the unmodified SnHTL photoanode. Finally, the SnHTL/p-NiFe interface showed the most favorable combination of high charge transfer rate (for $V \geq 1$ V) and slow recombination, leading to the performance enhancement expected when an adaptive SC/WOC junction is formed, showing the highest interfacial hole transfer efficiency (η_{WO}) of 75%.

Direct insights on the characteristics of hematite-based interfaces can be obtained also via transient photocurrent analysis (TPC), an informative, yet not routinely used, characterization technique. TPC consists in the excitation of the SC with a short laser pulse (usually in the 10^{-8} s time scale), which results in the photocurrent generation by the photoanode, recorded with fast chronoamperometric methods (typically with $10^{-6} - 10^{-4}$ s time resolution). The registered transient photocurrent features (shape and intensity) depend on the competition between charge separation and recombination, which are affected by the polarization of the photoelectrode. Thus, from the integrated photocurrent vs time decay profile, one could extract information about the amount of photocharge effectively transported and collected, as well as about the portion which is lost via trapping, slow recombination involving intragap states and so on. Fast recombination processes, occurring within < 1 ms time scales, cannot be usually observed by TPC, but they directly affect the overall amount of the extracted charge.

In particular, we have recently reported on the use of this technique in the characterization of the charge transfer dynamics in α-Fe_2O_3/$FeTiO_3$ composites, used for the first time to promote photoelectrochemical water oxidation [6]. In this work, the initial goal was to introduce Ti(IV) ions as dopants during the electrophoretic preparation of mesoporous hematite photoanodes [35]. By investigating the resulting electrodes by X-ray absorption fine structure (XAFS) and high resolution transmission electron microscopy (HR-TEM), we instead found

that Ti(IV) ions are incorporated in the form of surface layers of ilmenite ($FeTiO_3$). The resulting α-Fe_2O_3/$FeTiO_3$ interface was initially studied by transient absorption spectroscopy (TAS) and compared to the bare hematite counterpart (which does not contain any Ti ions).

As reported in Fig. 7, photogenerated holes (featuring a broad absorption band in the range 540–640 nm [55]) are rapidly (≪ ms) and more efficiently trapped in the α-Fe_2O_3/$FeTiO_3$ photoanode, resulting in a nearly doubled 580 nm absorption. The fate of the photogenerated carriers was further studied by means of TPC, allowing for the identification of two processes within two different time regimes. In particular, from the integration of the TPC trace (Fig. 8a) over time, the total charge vs time profile (reported in the inset) is obtained, from which we can identify (i) *Qgen*, i.e. the generated charge, net of fast recombination processes (which cannot be resolved on the experiment timescale); (ii) *Qrec*, i.e. charge lost due to slow recombination processes taking place via longer-lived trap states; and (iii) *Qcoll*, i.e. the actual collected charge, given by *Qgen* - |*Qrec*|.

While the applied bias dependence of *Qcoll* directly correlates with the J-V performances of the two investigated interfaces (see Fig. 8b), the *Qrec* values for α-Fe_2O_3 and α-Fe_2O_3/$FeTiO_3$ significantly varies. Indeed, as reported in Fig. 8c, for the bare hematite photoelectrode (black trace), the *Qrec* values are low (ca. 0.05 μC) and quite constant upon the applied bias range, suggesting that only a small fraction of holes survives fast recombination and can undergo slow recombination. On the other hand, the *Qrec* distribution for α-Fe_2O_3/$FeTiO_3$ photoanodes (red trace in Fig. 8c) displays a bell-shaped behavior in the range 0.6–1.4 V (dropping to 0 for V ≥ 1.4 V), speaking in favor of a higher population of holes being trapped in long-lived surface states induced by the presence of the $FeTiO_3$ phase. Indeed the ilmenite overlayer acts as a passivating agent for α-Fe_2O_3 deep traps, inducing also a greater number of oxygen vacancies (i.e. shallow donor states), which reduce bulk recombination. At the same time, it results in a strong depletion field that more effectively separates the photogenerated charges, favoring hole transfer to the electrolyte. On the other hand, the space charge built up in α-Fe_2O_3 photoelectrodes is not strong enough to guarantee efficient collection. It is worth noting that the same conclusions can be drawn also from the *Qrec* values normalized for the corresponding *Qgen* for the different interfaces (see inset of Fig. 8c).

Thus, our results enabled the identification and the understanding of a *n-n* heterojunction made of earth-abundant and non-toxic elements with enhanced photoelectrochemical performances. This kind of mechanistic insights are pivotal to gain knowledge on the dynamics of both the bare SC and of its modified/optimized versions, especially in view of a future rational design of new composite photoanodes with improved kinetics. In particular, "in operando" techniques should be preferred, since the behavior of the photoactive interface should be probed in the actual operation conditions (e.g. applied bias, presence of the electrolyte, simulated solar illumination, etc.)

4. Production of value-added chemicals via hematite-based PEC devices

Even if hematite is most frequently used as oxygen evolving photoanode in PEC set-ups for the overall water splitting, recently some examples of its use in alternative PECs, devoted to organic transformations, have started to appear [56–58]. This kind of approach is growing in interest, since the high oxidizing/reducing power that can be generated in illuminated PEC cells can be exploited to promote redox transformation of organic molecules to yield value-added products, under generally milder conditions with the respect to traditional organic synthesis methods involving chemical oxidants/reductants. As regarding PEC-mediated oxidations, the scene is currently dominated by the use of $BiVO_4$ and WO_3 photoanodes, which were employed for the oxidation of 5-hydroxymethylfurfural [59], benzylic alcohols [60,61], furan [62], as well as cyclohexane [63]. On the other hand, the use of hematite is still quite limited, but it is worth to be commented.

For example, the Durrant group reported on the mechanistic study of the selective PEC oxidation of methanol to formaldehyde on hematite photoanodes via photoinduced absorption spectroscopy and transient photocurrent measurements (Fig. 9a). This reaction was found to proceed with near unity Faradaic efficiency, while its rate was second order in the density of surface holes, and independent of the applied bias [58].

More recently, Mazzaro *et al.* reported on the oxidation of an acetonitrile solution of benzilamine to *N*-benzylidenebenzylamine, a valuable intermediate in organic synthesis, using Ti-doped hematite photoanodes [56]. By illuminating the electrode and applying an external bias (0.8 V vs the Standard Hydrogen Electrode, SHE), the concomitant production of ~150 μmol h^{-1} of H_2 is obtained at the cathode of the two compartment cell from the water reduction reaction (Fig. 9b).

Another interesting example of photoelectrochemical synthesis was recently reported by Hu et al., and involved the use of hematite photoanodes to promote the arene C—H amination reaction, aimed at synthesizing nitrogen-containing heterocycles relevant to drug discovery [57]. This reaction exploits holes photogenerated in hematite to oxidize electron-rich arenes, to give radical cations, followed by addition of nitrogen-containing nucleophiles. Interestingly, an unusual *ortho*-selectivity (up to 75% prevalence over the *para* isomer) is achieved for the pyrazole substitution of many aromatic substrates when the photoelectrochemical route is followed (Fig. 9c), compared to previously reported photoredox/electrochemical methods, mainly affording the *para* substitution. The photoelectrochemical route may exhibit this kind of regioselectivity due to hydrogen-bonding between the substrates and the hexafluoroisopropanol (HFIP) co-solvent, which may stabilize the

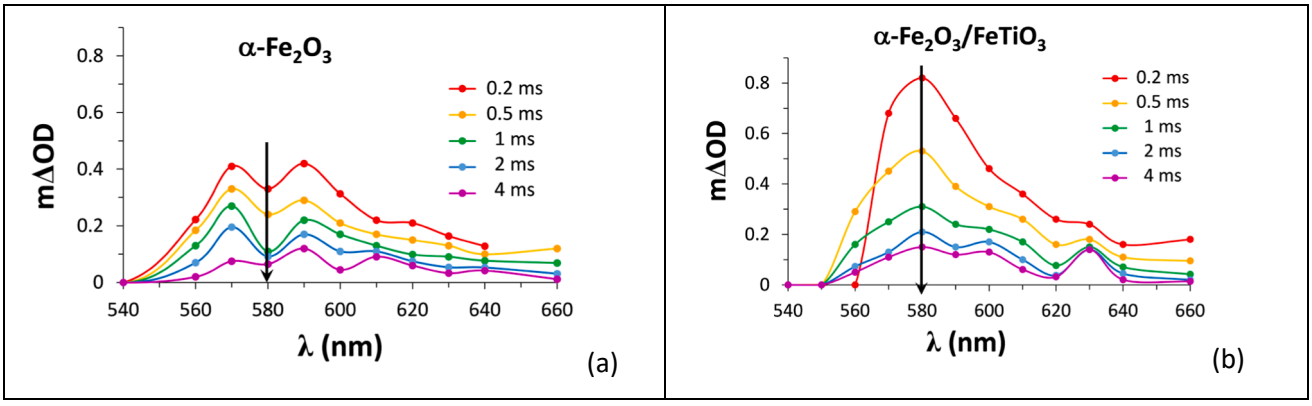

Fig. 7. Transient absorption spectra of mesoporous α-Fe_2O_3 (a) and α-Fe_2O_3 /$FeTiO_3$ (b) photoanodes at open-circuit potential (V_{OC}). Adapted with permission from [6] (Copyright 2020, American Chemical Society†).

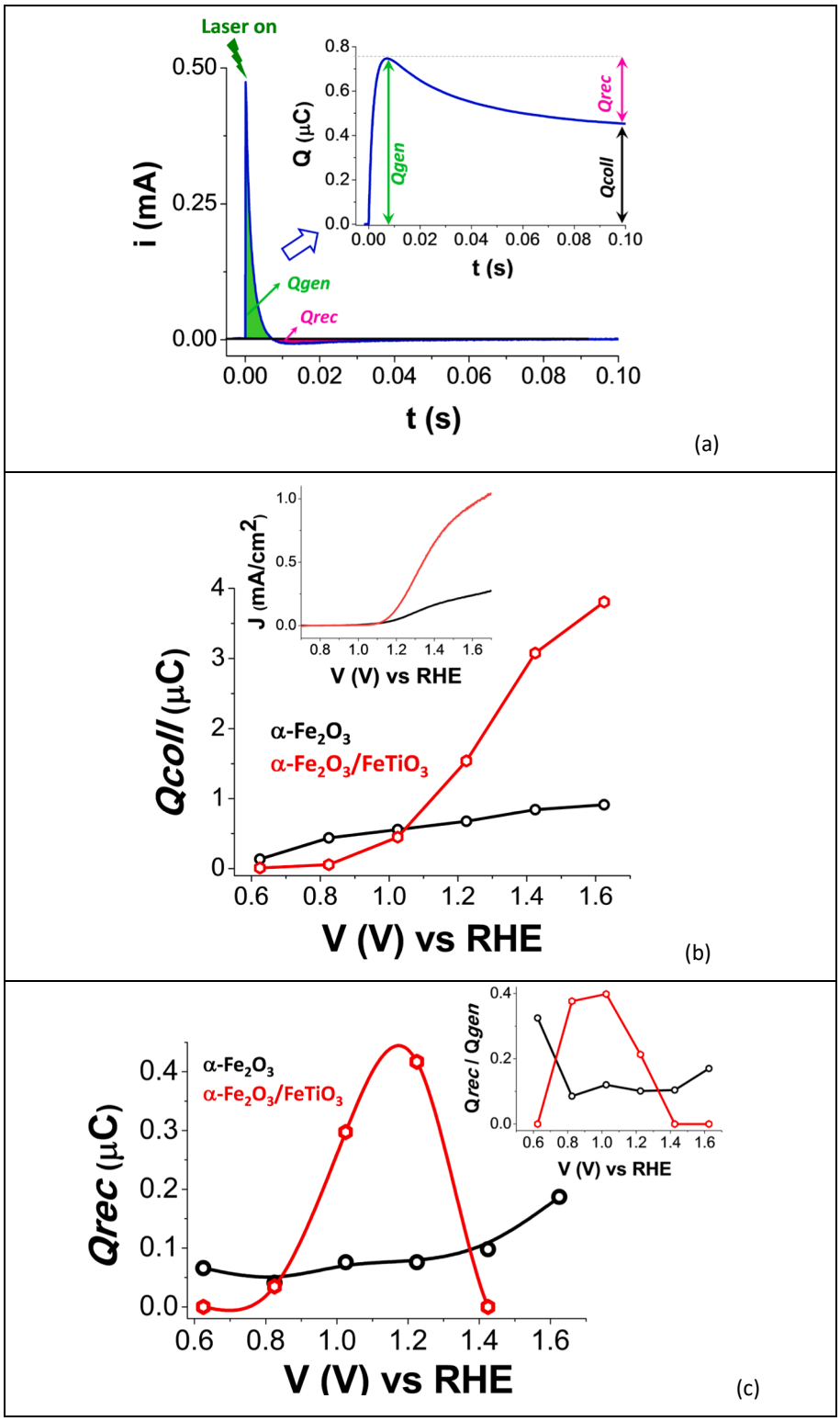

Fig. 8. (a) Typical TPC profile and its integration over time (inset), corresponding to the photogenerated charge. The contributions due to Q*gen*, Q*rec* and Q*coll* are indicated. (b-c) Applied bias dependence of Q*coll* (b) and Q*rec* (c) for α-Fe_2O_3 (black traces) and α-Fe_2O_3/$FeTiO_3$ (red traces) photoanodes. The corresponding J-V curves and the applied bias dependence of Q*rec*/Q*gen* are also reported (inset of b and c, respectively). Adapted with permission from [6] (Copyright 2020, American Chemical Society†).

substitution intermediate via N—H—F hydrogen bonding. This selectivity has been proved useful for the late stage modification with pyrazole, as an example of nucleophilic heterocycle, of pharmaceutical species, like muscle relaxants, antimicrobial agents and lipid lowering agents.

These works are thus paving the way for the production of value-added oxidation processes in industrial-scale photoreactors, exploiting the use of solar energy and of a cheap and widely available light harvesting material, like hematite. When compared to traditional organic synthesis, this kind of approach would also benefit from simplified work-up procedures, being the photoanode easily removable and reusable, making the overall process more sustainable. Furthermore, the product selectivity observed in some cases bode well for reduced waste production and work-up costs.

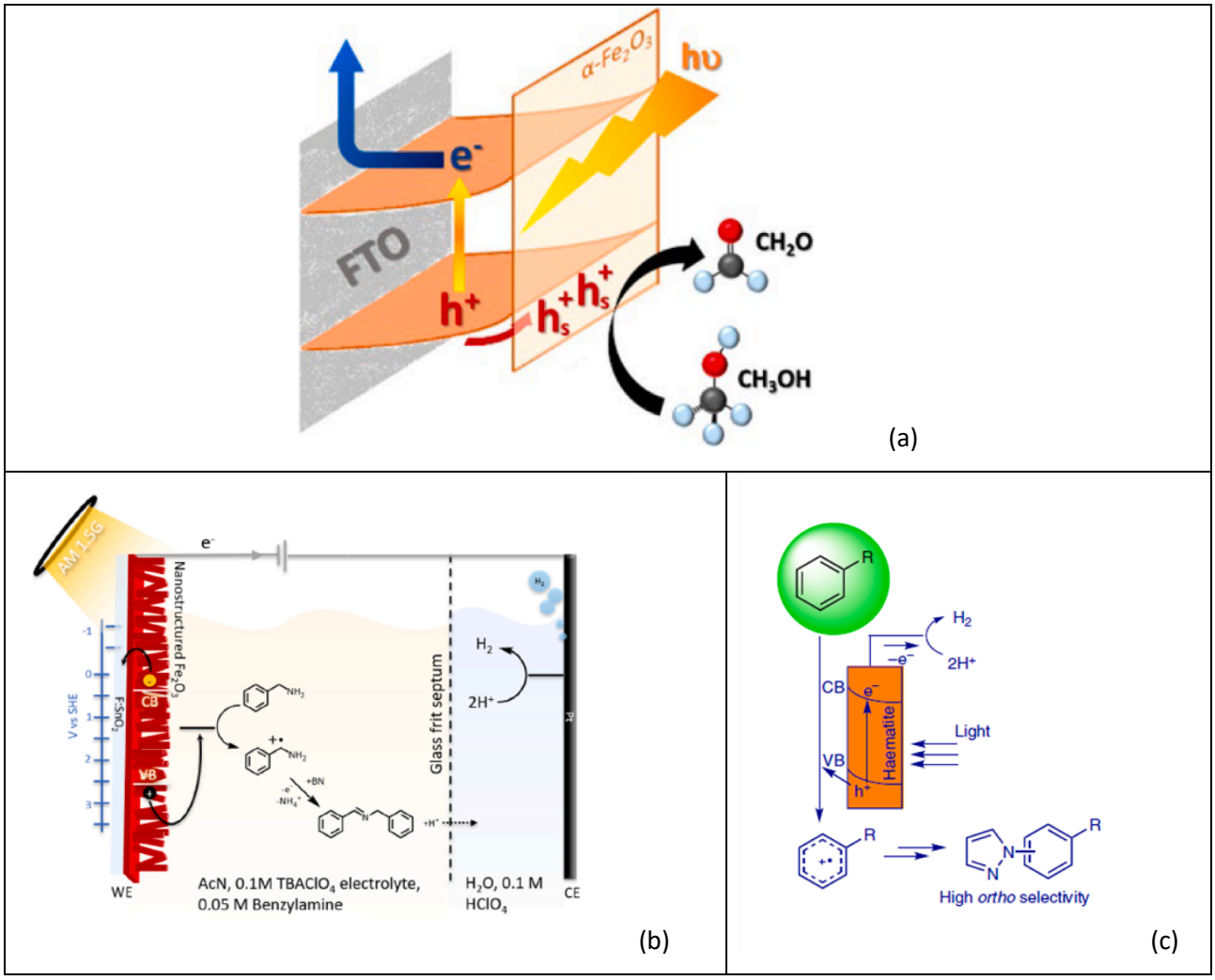

Fig. 9. Examples of application of hematite photoanodes in the photoelectrochemical (hole mediated) preparation of value-added chemicals: (a) Oxidative synthesis of formaldehyde from methanol (reproduced with permission from [58], Copyright 2017, American Chemical Society†); (b) Production of *N*-benzylidenebenzylamine starting from benzilamine (reproduced with permission from [56], Copyright 2019, Elsevier); (c) Decoration of electron rich arenes with nucleophilic nitrogen heterocycles (reproduced with permission from [57],Copyright 2019, Springer Nature).

5. Conclusions and outlook

In this short review, we have discussed some of the properties and the recent progresses involving the use of hematite, an environmentally friendly, earth abundant *n*-type semiconductor capable of harvesting a sizable portion of the solar spectrum. While these characteristics make hematite extremely attractive for solar energy conversion via photoelectrochemical processes, the poor mobility of charge carriers in α-Fe_2O_3 make its efficient exploitation rather problematic. Thus, viable strategies of increasing and optimizing the photoelectrochemical properties of hematite rely on the formation of thin films having highly porous structures allowing to enhance the hole percolation pathways to the electrolyte. At the same time, doping and formation of homo/heterointerfaces can be exploited to increase semiconductor conductivity, passivate intragap traps and increase the interfacial Schottky barrier, in order to direct the photoproduced minority carriers where scavenging by the electrolyte occurs. The surface modification of α-Fe_2O_3 with a water oxidation catalyst, often in the form of a metal (or mixed metal) oxide with low overpotential for oxygen evolution, has been shown to be instrumental in increasing hematite performance, but the details of the mechanisms acting at the heterointerface hosting the WOC are often not so straightforward to understand. Methods of investigation may thus include a combination of techniques, which rely on: (i) electrochemical impedance spectroscopy, in order to resolve the capacitive response of the interface in the frequency domain; (ii) the recording of photocurrent/photocharge transients produced by a fast pulsed light source; and (iii, when possible) the direct observation of the charge transfer dynamics by means of time resolved optical spectroscopy. This pool of techniques is instrumental, first of all, to gain a deeper understanding of bare hematite, whose photoelectrochemical performances are currently far below the thermodynamic maximum. This is an essential prerequisite towards the further optimization of hematite-based interfaces, allowing for the design of specific syntheses and/or post-functionalizations. At the same time, more insights on hematite behavior need to be studied using "in operando" techniques, i.e. probing the electrodes in the actual experimental conditions (e.g. under the application of an external bias and in the presence of the electrolyte). This is particularly needed for ultrafast spectroscopic experiments (usually carried out "ex situ", i.e. in air), which would provide important information on the early stage dynamics of charge transfer, and how they influence the ultimate reaction kinetics.

More investigations should also be aimed at probing the actual effect of the surface functionalization with water oxidation catalysts, as well as the effect of the surface states, and their mutual interaction. Theoretical simulations should also be performed, since their outcomes would guide in the material design, avoiding the exploration of manifold

experimental parameters/conditions. At the same time, low-cost fabrication methods for the deposition of high quality hematite films should be implemented also on large area substrates, in view of the production of real scale PEC-devices. To this end, the long-term stability of the photoactive interfaces in the operation conditions should be also probed.

In the final part of the short review, we have reported some inspiring examples of what we believe is one the most appealing application of photoelectrosynthetic cells, i.e. the solar driven oxidative chemistry aimed at the preparation of valued added chemicals of industrial/pharmaceutical interest. While still in its infancy, this approach could be the cleverest way to capitalize on the solar energy harvested by the photoelectrochemical device, where the production of useful chemicals at the photoanode is accompanied by the simultaneous production of hydrogen as a green fuel at the cathode of the cell.

CRediT authorship contribution statement

Serena Berardi: Conceptualization, Writing – original draft. **Vito Cristino:** Data curation, Visualization. **Carlo Alberto Bignozzi:** Writing – review & editing. **Silvia Grandi:** Data curation, Visualization. **Stefano Caramori:** Conceptualization, Writing – original draft.

Declaration of Competing Interest

The authors declare that they have no known competing financial interests or personal relationships that could have appeared to influence the work reported in this paper.

Acknowledgements

University of Ferrara (Italy) acknowledges financial support from Emilia Romagna Region (PNRR, D.M. 1061/2021) and H2020 Research Innovation Actions 2020-2024 “CONDOR”. This project has received funding from the European Union’s Horizon 2020 research and innovation programme, under grant agreement No 101006839.

References.

[1] K. Sivula, F. Le Formal, M. Grätzel, ChemSusChem 4 (2011) 432–449.
[2] F.E. Osterloh, Solar Energy for Fuels (2015) 105–142.
[3] F. Morin, Phys. Rev. 83 (1951) 1005.
[4] J.H. Kennedy, K.W. Frese Jr, J. Electrochem. Soc. 125 (1978) 709.
[5] D. Monllor-Satoca, M. Bärtsch, C. Fabrega, A. Genç, S. Reinhard, T. Andreu, J. Arbiol, M. Niederberger, J.R. Morante, Energy Environ. Sci. 8 (2015) 3242–3254.
[6] S. Berardi, J. Kopula Kesavan, L. Amidani, E.M. Meloni, M. Marelli, F. Boscherini, S. Caramori, L. Pasquini, ACS Appl. Mater. Interf. 12 (2020) 47435–47446.
[7] M. Orlandi, S. Berardi, A. Mazzi, S. Caramori, R. Boaretto, F. Nart, C.A. Bignozzi, N. Bazzanella, N. Patel, A. Miotello, ACS Appl. Mater. Interf. 11 (2019) 48002–48012.
[8] M. Orlandi, N. Dalle Carbonare, S. Caramori, C.A. Bignozzi, S. Berardi, A. Mazzi, Z. El Koura, N. Bazzanella, N. Patel, A. Miotello, ACS Appl. Mater. Interf. 8 (2016) 20003–20011.
[9] N. Dalle Carbonare, V. Cristino, S. Berardi, S. Carli, R. Argazzi, S. Caramori, L. Meda, A. Tacca, C.A. Bignozzi, ChemPhysChem 15 (2014) 1164–1174.
[10] Y. Ling, G. Wang, D.A. Wheeler, J.Z. Zhang, Y. Li, Nano Lett. 11 (2011) 2119–2125.
[11] Y.-S. Hu, A. Kleiman-Shwarsctein, A.J. Forman, D. Hazen, J.-N. Park, E. W. McFarland, Chem. Mater. 20 (2008) 3803–3805.
[12] C. Li, Z. Luo, T. Wang, J. Gong, Adv. Mater. 30 (2018) 1707502.
[13] P.-Y. Tang, L.-J. Han, F.S. Hegner, P. Paciok, M. Biset-Peiró, H.-C. Du, X.-K. Wei, L. Jin, H.-B. Xie, Q. Shi, T. Andreu, M. Lira-Cantú, M. Heggen, R.E. Dunin-Borkowski, N. López, J.R. Galán-Mascarós, J.R. Morante, J. Arbiol, Adv. En. Mater. 9 (2019) 1901836.
[14] F.S. Hegner, D. Cardenas-Morcoso, S. Giménez, N. López, J.R. Galan-Mascaros, ChemSusChem 10 (2017) 4552–4560.
[15] M.G. Ahmed, T.A. Kandiel, A.Y. Ahmed, I. Kretschmer, F. Rashwan, D. Bahnemann, J. Phys. Chem. C 119 (2015) 5864–5871.
[16] K.C. Bedin, D.N. Muche, M.A. Melo Jr, A.L. Freitas, R.V. Gonçalves, F.L. Souza, ChemCatChem 12 (2020) 3156–3169.
[17] D. Chen, Z. Liu, S. Zhang, Appl. Catal. B 265 (2020), 118580.
[18] S. Zhang, Z. Liu, D. Chen, W. Yan, Appl. Catal. B 277 (2020), 119197.
[19] D. Chen, Z. Liu, Z. Guo, M. Ruan, W. Yan, ChemSusChem 12 (2019) 3286–3295.
[20] X. Yang, R. Liu, C. Du, P. Dai, Z. Zheng, D. Wang, ACS Appl. Mater. Interf. 6 (2014) (2011) 12005–12011.
[21] F. Le Formal, N. Tetreault, M. Cornuz, T. Moehl, M. Grätzel, K. Sivula, Chem. Sci. 2 (2011) 737–743.
[22] F. Le Formal, K. Sivula, M. Grätzel, J. Phys. Chem. C 116 (2012) 26707–26720.
[23] T. Hisatomi, F. Le Formal, M. Cornuz, J. Brillet, N. Tétreault, K. Sivula, M. Grätzel, Energy Environ. Sci. 4 (2011) 2512–2515.
[24] L. Palmolahti, H. Ali-Löytty, R. Khan, J. Saari, N.V. Tkachenko, M. Valden, J. Phys. Chem. C 124 (2020) 13094–13101.
[25] J. Li, W. Wan, C.A. Triana, H. Chen, Y. Zhao, C.K. Mavrokefalos, G.R. Patzke, Nat. Commun. 12 (2021) 1–9.
[26] B. Klahr, S. Gimenez, F. Fabregat-Santiago, T. Hamann, J. Bisquert, J. Am. Chem. Soc. 134 (2012) 4294–4302.
[27] L. Vayssieres, N. Beermann, S.-E. Lindquist, A. Hagfeldt, Chem. Mater. 13 (2001) 233–235.
[28] Y. Yang, M. Forster, Y. Ling, G. Wang, T. Zhai, Y. Tong, A.J. Cowan, Y. Li, Angew. Chem. Int. Ed. 55 (2016) 3403–3407.
[29] J.-W. Jang, C. Du, Y. Ye, Y. Lin, X. Yao, J. Thorne, E. Liu, G. McMahon, J. Zhu, A. Javey, Nat. Commun. 6 (2015) 1–5.
[30] O. Zandi, A.R. Schon, H. Hajibabaei, T.W. Hamann, Chem. Mater. 28 (2016) 765–771.
[31] L. Wang, C.-Y. Lee, P. Schmuki, Electrochim. Acta 91 (2013) 307–313.
[32] M. Khalil, J. Yu, N. Liu, R.L. Lee, J. Nanopart. Res. 16 (2014) 1–10.
[33] A. Kay, I. Cesar, M. Grätzel, J. Am. Chem. Soc. 128 (2006) 15714–15721.
[34] H. Zhu, Y. Zhang, J. Zhu, Y. Li, S. Jiang, N. Wu, Y. Wei, J. Zhou, Y. Song, J. Mater. Chem. A 8 (2020) 22929–22937.
[35] N. Dalle Carbonare, R. Boaretto, S. Caramori, R. Argazzi, M. Dal Colle, L. Pasquini, R. Bertoncello, M. Marelli, C. Evangelisti, C.A. Bignozzi, Molecules 21 (2016) 942.
[36] A.F. Gualtieri, P. Venturelli, Am. Mineral. 84 (1999) 895–904.
[37] J. Brillet, M. Gratzel, K. Sivula, Nano Lett. 10 (2010) 4155–4160.
[38] S.C. Warren, K. Voïtchovsky, H. Dotan, C.M. Leroy, M. Cornuz, F. Stellacci, C. Hébert, A. Rothschild, M. Grätzel, Nat. Mater. 12 (2013) 842–849.
[39] G. Pike, C.H. Seager, J. Appl. Phys. 50 (1979) 3414–3422.
[40] Y. Li, N. Guijarro, X. Zhang, M.S. Prevot, X.A. Jeanbourquin, K. Sivula, H. Chen, Y. Li, ACS Appl. Mater. Interf. 7 (2015) 16999–17007.
[41] E. Yablonovitch, Phys. Rev. Lett. 58 (1987) 2059–2062.
[42] S. John, Phys. Rev. Lett. 58 (1987) 2486.
[43] P. Peerakiatkhajohn, J.H. Yun, H. Chen, M. Lyu, T. Butburee, L. Wang, Adv. Mater. 28 (2016) 6405–6410.
[44] Y. Zhang, S. Jiang, W. Song, P. Zhou, H. Ji, W. Ma, W. Hao, C. Chen, J. Zhao, Energy Environ. Sci. 8 (2015) 1231–1236.
[45] X. Zhang, P. Klaver, R. van Santen, M. Van De Sanden, A. Bieberle-Hütter, J. Phys. Chem. C 120 (2016) 18201–18208.
[46] S. Zou, M.S. Burke, M.G. Kast, J. Fan, N. Danilovic, S.W. Boettcher, Chem. Mater. 27 (2015) 8011–8020.
[47] P. Dias, L. Andrade, A. Mendes, Nano Energy 38 (2017) 218–231.
[48] J. Qiu, H. Hajibabaei, M.R. Nellist, F.A.L. Laskowski, T.W. Hamann, S. W. Boettcher, ACS Cent Sci. 3 (2017) 1015–1025.
[49] F. Lin, S.W. Boettcher, Nat. Mater. 13 (2014) 81–86.
[50] T. Yao, X. An, H. Han, J.Q. Chen, C. Li, Adv. En. Mater. 8 (2018) 1800210.
[51] M.B. Stevens, L.J. Enman, A.S. Batchellor, M.R. Cosby, A.E. Vise, C.D. Trang, S. W. Boettcher, Chem. Mater. 29 (2017) 120–140.
[52] M.S. Burke, S. Zou, L.J. Enman, J.E. Kellon, C.A. Gabor, E. Pledger, S.W. Boettcher, J. Phys. Chem. Lett. 6 (2015) 3737–3742.
[53] Z. Guo, Z. Liu, Dalton Trans. 50 (2021) 1983–1989.
[54] K.G. Upul Wijayantha, S. Saremi-Yarahmadi, L.M. Peter, Phys. Chem. Chem. Phys. 13 (2011) 5264–5270.
[55] M. Barroso, S.R. Pendlebury, A.J. Cowan, J.R. Durrant, Chem. Sci. 4 (2013) 2724–2734.
[56] R. Mazzaro, S. Boscolo Bibi, M. Natali, G. Bergamini, V. Morandi, P. Ceroni, A. Vomiero, Nano Energy 61 (2019) 36–46.
[57] L. Zhang, L. Liardet, J. Luo, D. Ren, M. Grätzel, X. Hu, Nat. Catal. 2 (2019) 366–373.
[58] C.A. Mesa, A. Kafizas, L. Francàs, S.R. Pendlebury, E. Pastor, Y. Ma, F. Le Formal, M.T. Mayer, M. Grätzel, J.R. Durrant, J. Am. Chem. Soc. 139 (2017) 11537–11543.
[59] H.G. Cha, K.-S. Choi, Nat. Chem. 7 (2015) 328–333.
[60] T. Li, T. Kasahara, J. He, K.E. Dettelbach, G.M. Sammis, C.P. Berlinguette, Nat. Commun. 8 (2017) 390.
[61] H. Tateno, Y. Miseki, K. Sayama, ChemElectroChem 4 (2017) 3283–3287.
[62] H. Tateno, Y. Miseki, K. Sayama, Chem. Commun. 53 (2017) 4378–4381.
[63] H. Tateno, S. Iguchi, Y. Miseki, K. Sayama, Angew. Chem. Int. Ed. 57 (2018) 11238–11241.